COBEM 2023 27TH INTERNATIONAL CONGRESS OF MECHANICAL ENGINEERING

ABCM Brazilian Society of Mechanical Sciences and Engineering
27th ABCM International Congress of Mechanical Engineering
December 04-08, 2023, Florianópolis-SC, Brazil

COB-2023-2128
MODELING OF FUNCTIONALLY GRADED MATERIAL (FGM) PLATES BENDING VIA GFEM

Bruno Pereira Santos
Paulo de Tarso R. Mendonça
Dept. of Mechanical Engineering, Federal University of Santa Catarina (UFSC)
Centro Tecnológico, Campus Universitário, Trindade, 88040-900, Santa Catarina, Brazil
bruno.pe.santos1@gmail.com, mendonca@grante.ufsc.br

Abstract. *This paper presents a formulation of Generalized Finite Element Method (GFEM) capable of analyzing Functionally Graded Material (FGM) plates subjected to mechanical loads in high gradient thermal field environments. A Reissner-Mindlin's first-order shear theory model for composite materials was used as foundation for the developed method. Given the boundary conditions and base materials' thermomechanical properties, this formulation uses Finite Difference Method to solve the steady-state heat conduction problem along the structure's thickness and obtain the temperature field of the plate. Temperature dependence of thermal conductivities, elasticity moduli and thermal expansion coefficients is considered, and stiffness matrices and force vectors are computed via numerical integration along the plate's thickness. The GFEM model considers a linear stress-strain relationship, using three-noded triangular elements and Shephard's Partitions of Unit with smooth approximation functions enriched by linearly independent polynomials. Weak thermomechanical coupling is considered and the elastic problem's solution is found applying Newton-Raphson's method. As well as the formulation developed, this report shows its application in the solution of a plate-bending problem under thermal gradient and mechanical loading effects. A comparison between the numerical solution and an analytical first-order counterpart validates the method's implementation, obtaining distributed relative errors based on a L_2-norm with order under $10^{-4}\%$ for Mindlin's displacements.*

Keywords: *Functionally Graded Material, Composite Materials, Generalized Finite Element Method, Reissner-Mindlin's model.*

1. INTRODUCTION

First idealized in the early 1970s by Bever and Duwez (1972) and manufactured in 1987 by the Science and Technology Agency, of Japan (Koizumi and Niino, 1995), Functionally Graded Materials (FGM) have proved themselves extremely valuable in applications that demand operation under both mechanical loads and harsh thermal gradients. Among other fields, their capacity of maintaining integrity under harsh thermal conditions has become a fundamental asset in the aerospace industry, being used to shield space shuttles and artificial satellites during atmosphere exit and reentry (Swaminathan and Sangeetha, 2017)

Due to the increasing usage of FGM in industry, and being this a relatively new kind of material, it is important to further develop analysis models focused on representing the coupling of mechanical and thermal effects in this kind of composite. Much research has been done in the area, namely by authors such as Reddy (1998) and Park and Kim (2006), but there are still many topics that need to be researched and understood.

Parallel to this, in recent years, GFEM has risen as a valuable asset in computational assisted engineering. This alternative to conventional FEM and meshless methods is capable of efficient boundary value problem solving, having less dependency on mesh geometry than conventional FEM and lower computational cost than the main meshless methods as well as easier implementation of Dirichlet boundary conditions. Among other researchers, Barcellos *et al.* (2009) was responsible for important advances in this area, having developed a C^k continuous formulation of the method. Given that GFEM may be a valuable tool in the analysis of complex structures and materials, this paper aims to present and inspire further development in the development of GFEM models for FGM plates.

2. THEORETICAL FORMULATION

2.1 FGM Properties

Following the work of Reddy (2000), Material properties' gradation along plate thickness can be suitably described by a weighted mean and a proposed material distribution, chosen here as the power law presented in Eq. (1). $V_c(z)$ is the volume fraction of ceramic material at a certain coordinate z, P_c and P_m the properties of the metallic and ceramic

materials and n the FGM's distribution parameter.

$$P(z) = (P_c - P_m)V_c + P_m,$$
$$V_c(z) = \left(\frac{1}{2} + \frac{z}{H}\right)^n \qquad n \geq 0, \tag{1}$$

It's important to reinforce that, although the materials are referred to in this study as 'metal' and 'ceramic' for notation simplicity, the formulation proposed is applicable for any pair of isotropic materials. Furthermore, for the purposes of this study, ν and α are considered to be constant for both materials, while E and k are considered to be temperature dependent, following Eq. (2) (Park and Kim, 2006).

$$P_m(T) \text{ (or } P_c(T)) \ = P_o(P_{-1}T^{-1} + 1 + P_1T + P_2T^3 + P_3T^3) \tag{2}$$

Notably, despite the composite nature of the plate's structure, each point of it behaves as an isotropic material. Figure 1 represents the FGM's geometry and composition, while Fig. 2 presents the material distribution along plate thickness for different values of distribution parameter n.

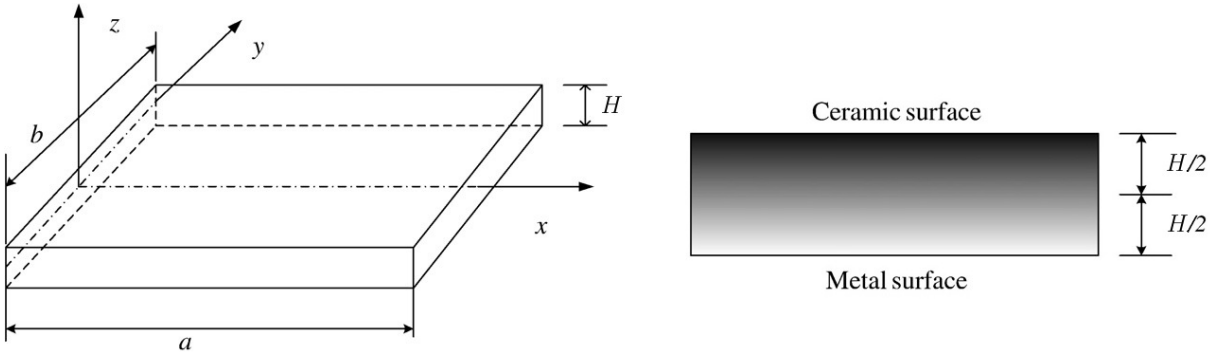

Figure 1. FGM plate's geometry and coordinate system. Source: Lee *et al.* (2010), adapted

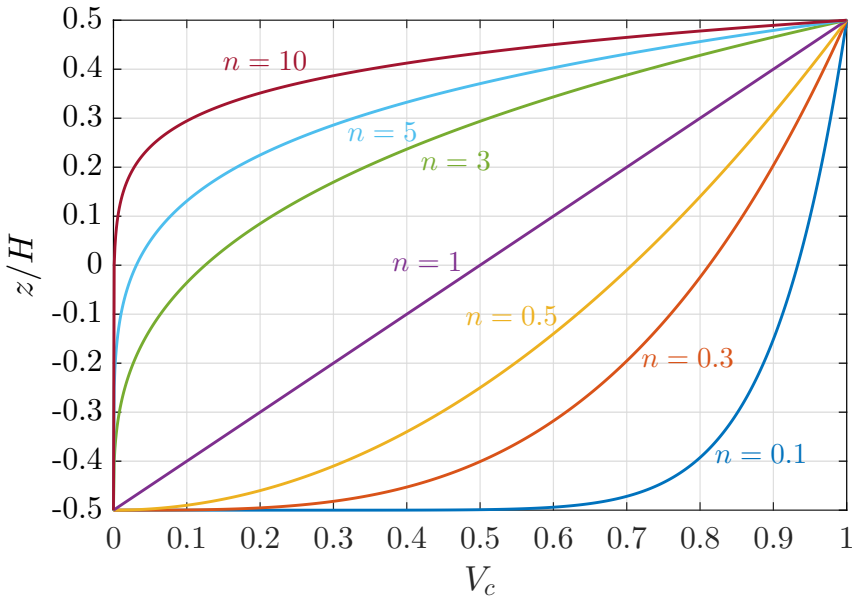

Figure 2. Volumetric fraction of ceramic material along the plate's thickness for different values of n, showing the distribution parameter's influence on the FGM's composition.

2.2 Mechanical behavior

Widely used in engineering analysis and commercial FEM software, Reissner-Mindlin's plate theory is currently among the main First-order Shear Deformation Theories (FSTD). Equation (3) describes the movement relations charac-

teristic to this FSTD (Mendonça, 2019).

$$\begin{aligned} u(x,y,z) &= u^o(x,y) + z\phi_x(x,y), \\ v(x,y,z) &= v^o(x,y) + z\phi_y(x,y), \\ w(x,y,z) &= w(x,y) \end{aligned} \tag{3}$$

where u, v and w are the coordinates of a point in the deformed configuration, index $(\ )^o$ represents the position of the plate's reference plane and ϕ_x e ϕ_y are cross-section rotations around axis x and y.

$$\phi_x = \frac{\partial u}{\partial z}, \qquad \phi_y = \frac{\partial v}{\partial z} \tag{4}$$

The following constitutive equations might then be used to describe the Mindlin plate's bending behavior under mechanical loads:

$$\left\{ \begin{array}{c} \mathbf{N} \\ \mathbf{M} \end{array} \right\} = \left[\begin{array}{cc} \mathbf{A} & \mathbf{B} \\ \mathbf{B} & \mathbf{D} \end{array} \right] \left\{ \begin{array}{c} \boldsymbol{\varepsilon}^o \\ \boldsymbol{\kappa} \end{array} \right\}, \tag{5}$$

$$\mathbf{Q}_t = \mathbf{E}\boldsymbol{\gamma}_c,$$

where

$$\mathbf{A} = \int_{-H/2}^{H/2} \mathbf{Q}\, dz, \quad \mathbf{B} = \int_{-H/2}^{H/2} z\mathbf{Q}\, dz, \quad \mathbf{D} = \int_{-H/2}^{H/2} z^2\mathbf{Q}\, dz \tag{6}$$

and

$$\mathbf{E} = k \int_{-H/2}^{H/2} \mathbf{e}\, dz, \qquad \mathbf{e} = \left[\begin{array}{cc} C_{44}^x & C_{45}^x \\ C_{45}^x & C_{55}^x \end{array} \right] \tag{7}$$

In the analysis of laminated composite Eqs. (6) and (7) and generally computed through the sum of layer-wise components. However, as FGM aren't divided in layers and their properties aren't easily computed by analytic integration, these matrices must generally be calculated by numeric integration processes or other approximation methods. This paper uses Simpson's 3/8 rule to compute these and other through-thickness integrals, dividing the coordinate's domain into a series of sub-intervals and integrating each one by cubic polynomial approximations.

Considerations about deformations due to effect of the thermal field will be made in Section 2.4

2.3 Temperature field distribution

The temperature field $T(z)$ is given by the solution of a one-dimensional steady-state heat conduction problem, with prescribed temperatures on the boundaries and no internal heat sources. Equation (8) presents this problem (Reddy, 2000), being $k(z,T)$ the FGM's thermal conductivity. .

$$\begin{aligned} -\frac{d}{dz}\left(k(z,T)\frac{dT}{dz}\right) &= 0 \qquad \text{in } z \in (-H/2, H/2), \\ T(-H/2) &= T_m, \\ T(H/2) &= T_c, \end{aligned} \tag{8}$$

Due to the dependency that $k(z,T)$ has on the distribution of ceramic and metallic material in the plate, an analytical solution for an arbitrary value of n is not possible. Therefore, this solution is usually obtained numerically, through methods such as the Finite Difference Method (FDM), used in this study. Furthermore, as this paper considers the effect of temperature in the conductivity $k(z,T)$, an iterative procedure had to be adopted to compute $T(z)$. The L_2-norm loss function was used to evaluate convergence.

2.4 Thermal effects in bending

Since FGM are considered to be isotropic at each coordinate z, the stress-strain relationship for the FSTD model can be expressed by Eq. (9).

$$\left\{ \begin{array}{c} \sigma_x \\ \sigma_y \\ \tau_{xy} \end{array} \right\} = \left[\begin{array}{ccc} Q_{11} & Q_{12} & \\ Q_{12} & Q_{22} & \\ & & Q_{66} \end{array} \right] \left\{ \begin{array}{c} \varepsilon_x - \alpha\Delta T \\ \varepsilon_y - \alpha\Delta T \\ \gamma_{xy} \end{array} \right\} \quad \rightarrow \quad \boldsymbol{\sigma} = \mathbf{Q}\left(\boldsymbol{\varepsilon} - {}^{\mathcal{T}}\boldsymbol{\varepsilon}\right) \tag{9}$$

where ${}^{\mathcal{T}}\varepsilon = \alpha\Delta T\mathbf{1}$ is the strain component due to thermal dilation, and $\mathbf{1} = \{1,1,0\}^T$. Transverse shear equations aren't affected by temperature effects:

$$\left\{ \begin{array}{c} \tau_{yz} \\ \tau_{xz} \end{array} \right\} = \left[\begin{array}{cc} Q_{44} & \\ & Q_{55} \end{array} \right] \left\{ \begin{array}{c} \gamma_{yz} \\ \gamma_{xz} \end{array} \right\} \quad \rightarrow \quad \boldsymbol{\tau} = \mathbf{Q}^s\boldsymbol{\gamma} \tag{10}$$

Isotropic behavior determines that $Q_{11} = Q_{22} = E/(1-v^2)$, $Q_{12} = vQ_{11}$, $Q_{66} = E/2(1+v)$, and $Q_{44} = Q_{55} = E/2(1+v)$.

Given the constitutive equation described by Eq. (5), it is true for FSTD that:

$$\boldsymbol{\varepsilon} = \boldsymbol{\varepsilon}^o + z\boldsymbol{\kappa} \tag{11}$$

A constitutive equation for FGM under thermomechanical effects can be obtained from the definition of in-plane and moment force resultants, described in Eq. (12).

$$\mathbf{N} = \int_{-H/2}^{H/2} \boldsymbol{\sigma}\, dz \quad \text{and} \quad \mathbf{M} = \int_{-H/2}^{H/2} \boldsymbol{\sigma} z\, dz. \tag{12}$$

Applying Eqs. (9) and (11) to the in-plane force resultant in Eq. (12),

$$\mathbf{N} = \underbrace{\int_{-H/2}^{H/2} \mathbf{Q}\, dz\boldsymbol{\varepsilon}^o}_{\mathbf{A}} + \underbrace{\int_{-H/2}^{H/2} z\mathbf{Q}\, dz\boldsymbol{\kappa}}_{\mathbf{B}} - \underbrace{\int_{-H/2}^{H/2} \mathbf{Q}\, {}^{\mathcal{T}}\boldsymbol{\varepsilon}\, dz}_{{}^{\mathcal{T}}\mathbf{N}} \tag{13}$$

Similarly, for the moment force resultant:

$$\mathbf{M} = \underbrace{\int_{-H/2}^{H/2} \mathbf{Q} z\, dz\boldsymbol{\varepsilon}^o}_{\mathbf{B}} + \underbrace{\int_{-H/2}^{H/2} z^2\mathbf{Q}\, dz\boldsymbol{\kappa}}_{\mathbf{D}} - \underbrace{\int_{-H/2}^{H/2} \mathbf{Q}\, {}^{\mathcal{T}}\boldsymbol{\varepsilon} z\, dz}_{{}^{\mathcal{T}}\mathbf{M}} \tag{14}$$

The thermal components in Eqs. (14) and (13) are given by:

$${}^{\mathcal{T}}\mathbf{N} = \underbrace{\int_{-H/2}^{H/2} \mathbf{Q}\alpha\Delta T\, dz\mathbf{1}}_{{}^0\mathbf{Q}} = {}^0\mathbf{Q}\mathbf{1} \quad \text{and} \quad {}^{\mathcal{T}}\mathbf{M} = \underbrace{\int_{-H/2}^{H/2} \mathbf{Q}\alpha\Delta T z\, dz\mathbf{1}}_{{}^1\mathbf{Q}} = {}^1\mathbf{Q}\mathbf{1}. \tag{15}$$

Hence, the FGM plate's constitutive relation becomes:

$$\left\{ \begin{array}{c} \mathbf{N} \\ \mathbf{M} \end{array} \right\} = \left[\begin{array}{cc} \mathbf{A} & \mathbf{B} \\ \mathbf{B} & \mathbf{D} \end{array} \right] \left\{ \begin{array}{c} \boldsymbol{\varepsilon}^o \\ \boldsymbol{\kappa} \end{array} \right\} - \left\{ \begin{array}{c} {}^{\mathcal{T}}\mathbf{N} \\ {}^{\mathcal{T}}\mathbf{M} \end{array} \right\}, \text{ where } \left\{ \begin{array}{c} {}^{\mathcal{T}}\mathbf{N} \\ {}^{\mathcal{T}}\mathbf{M} \end{array} \right\} = \left\{ \begin{array}{c} {}^0\mathbf{Q} \\ {}^1\mathbf{Q} \end{array} \right\} \mathbf{1}. \tag{16}$$

It's noticeable that this relation is formally the same used for anisotropic laminates. However, the procedure for computing the constitutive matrices $\mathbf{A}$, $\mathbf{B}$, $\mathbf{D}$, ${}^0\mathbf{Q}$ e ${}^1\mathbf{Q}$ is different and must be done via numeric integration.

2.5 GFEM applied to FGM

As presented by Mendonça (2019), from the matrix equation that represents the approximated form of Principle of Virtual Work (PVW) for FSTD plates it is possible to obtain, in compact notation,

$$[\mathbf{K}_f + \mathbf{K}_c]\,\mathbf{U} = \mathbf{F} \tag{17}$$

being $\mathbf{U}$ the nodal displacement vector, $\mathbf{F}$ the nodal force vector, and $\mathbf{K}_f$ and $\mathbf{K}_c$ stiffness matrices.

Thermal deformation introduces a new force component, defined in Eq. (18), which must be added to the vector representing mechanical loads in order to form the nodal force vector $\mathbf{F}$.

$${}^{\mathcal{T}}\mathbf{F} = \int_\Omega \mathbf{B}_f^T \left\{ \begin{array}{c} {}^{\mathcal{T}}\mathbf{N} \\ {}^{\mathcal{T}}\mathbf{M} \end{array} \right\} d\Omega, \tag{18}$$

Therefore, Eq. (17) becomes:

$$[\mathbf{K}_f + \mathbf{K}_c]\,\mathbf{U} = {}^m\mathbf{F} + {}^{\mathcal{T}}\mathbf{F} \tag{19}$$

The usage of FEM shape functions as a Partition of Unit (PU) that can be enriched by a set of linearly independent functions defines GFEM. Thus, it is possible to increase their capability of representing solutions without the need of increasing complexity and number of elements. For this study, polynomial enrichment functions were used.

3. NUMERICAL RESULTS

Two FGM problems were analyzed to validate the GFEM formulation developed and analytical solutions were used to verify numerical results. In both cases, the square plates where divided into a regular mesh of 128 triangular elements with linear shape functions, and GFEM enrichment was performed through the usage of quartic polynomial functions. The solutions were obtained by using Newton-Raphson's method.

3.1 Material properties

The materials adopted to compose the FGM plate were stainless steel and zirconia. Both materials were considered to have Poisson ratio $\nu = 0.3$ and temperature-independent thermal expansion coefficients $\alpha_m = 1.682 \times 10^{-5}$ K^{-1} and $\alpha_c = 3.013 \times 10^{-5}$ K^{-1}. Elasticity moduli and thermal conductivities were considered to behave as described by Eq. (2) and their coefficients are presented at Table 1 (Reddy, 1998).

Table 1. FGM plate's temperature-dependent material properties

Property	P_0	P_{-1}	P_1	P_2	P_3
E_m (Pa)	201.04×10^9	0	3.079×10^{-4}	-6.534×10^{-7}	0
E_c (Pa)	244.27×10^9	0	-1.371×10^{-3}	-1.214×10^{-6}	-3.681×10^{-10}
k_m (W/mK)	15.379	0	-1.264×10^{-3}	2.092×10^{-6}	-7.223×10^{-10}
k_c (W/mK)	1.7000	0	1.276×10^{-4}	6.648×10^{-8}	0

3.2 Nondimensionalization

A nondimensionalization procedure was used to simplify the notation of geometry and displacement results. Thus, nondimensional displacement are obtained as

$$\bar{\delta} = \frac{\delta E_c H^3}{q_o a^2 b^2}, \tag{20}$$

where δ refers to the displacements u, v or w. The dimensions of the rectangular plate are a, b and H and q_o is the maximum load value. Midlin's displacements ψ_x and ψ_y are by definition nondimensional and therefore weren't modified.

Normalization of the plate's geometry is used, as per

$$\bar{x} = \frac{x}{a}, \qquad \bar{y} = \frac{y}{b} \qquad \text{e} \qquad \bar{z} = \frac{z}{H}. \tag{21}$$

From Eq. (21), the domains $\bar{x}, \bar{y} \in [0, 1]$ and $\bar{z} \in \left[-\frac{1}{2}, +\frac{1}{2}\right]$ are obtained.

3.3 Bending of square Mindlin FGM plate under thermal and mechanical loads

A square plate with length $L = 0.5$ m, thickness $H = 0.05$ m and distribution coefficient $n = 2.0$ was considered to be simply supported on its edges. Top and bottom temperatures were assumed as $T_c = 800$K and $T_m = 300$K and deformation was considered to be caused simultaneously by thermal dilation and by a sinusoidal load in z-direction, represented by Eq. (22), in which a value $q_o = 10^5$ Pa was considered.

$$q(x, y) = q_o \sin\frac{\pi x}{L_x} \sin\frac{\pi y}{L_y} \tag{22}$$

Additionally, in order to simplify the problem and enable the calculation of an exact analytical solution to be used as reference for analysis of the GFEM model's behavior, additional restrictions were considered in the boundaries of the structure, as follows.

In $x = 0$ and $x = a, \forall y$

$$\left\| \begin{array}{ll} w(x, y) = 0, & v^o(x, y) = 0, \\ M_x(x, y) = -\,^{\mathcal{T}} M_x, & N_x(x, y) = -\,^{\mathcal{T}} N_x, \end{array} \right. \tag{23}$$

and in the edges $y = 0$ and $y = b, \forall x$,

$$\left\| \begin{array}{ll} w(x, y) = 0, & u^o(x, y) = 0, \\ M_y(x, y) = -\,^{\mathcal{T}} M_y, & N_y(x, y) = -\,^{\mathcal{T}} N_y. \end{array} \right. \tag{24}$$

Thus, in the absence of a thermal gradient, the problem is reduced to a simply supported case. However, if thermal effects are present, flexural and normal loads appear on the edges of the plate.

The exact solution for the presented problem's displacements is

$$\left\| \begin{array}{l} u^o = U_{mn} \cos \bar{m}x \sin \bar{n}y, \\ v^o = V_{mn} \sin \bar{m}x \cos \bar{n}y, \\ w^o = W_{mn} \sin \bar{m}x \sin \bar{n}y, \\ \psi_x = \Psi_{xmn} \cos \bar{m}x \sin \bar{n}y, \\ \psi_y = \Psi_{ymn} \sin \bar{m}x \cos \bar{n}y. \end{array} \right. \tag{25}$$

Considering the values defined, the nondimensional analytical solution is

$$\left\{ \begin{array}{c} \bar{U}_{mn} \\ \bar{V}_{mn} \\ \bar{W}_{mn} \\ \Psi_{xmn} \\ \Psi_{ymn} \end{array} \right\} = \left\{ \begin{array}{c} -1.9138 \cdot 10^{-4} \\ -1.9138 \cdot 10^{-4} \\ 3.7785 \cdot 10^{-2} \\ -4.6044 \cdot 10^{-5} \\ -4.6044 \cdot 10^{-5} \end{array} \right\}.$$

Figure 3 represents material distribution over thickness and the temperature field computed with FDM.

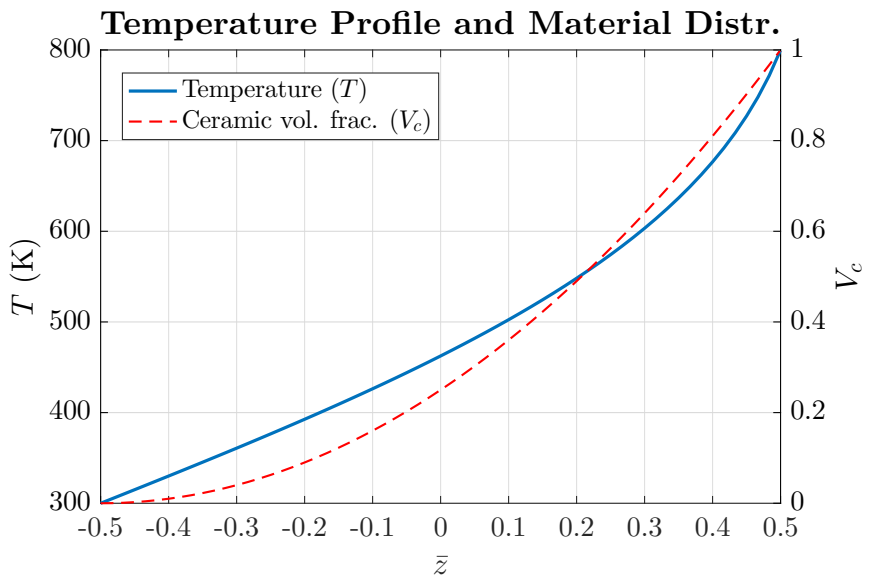

Figure 3. Volumetric fraction of ceramic $V_c(z)$ and temperature field $T(z)$ over plate's thickness

Figure 4 shows the results obtained using GFEM (due to the orthogonal symmetry of the problem, v^o and ψ_y^o possess behavior equivalent to that shown for u^o and ψ_x^o). An analytical solution was created and used as reference to calculate the errors of the numerical model and its results may be observed in superposition to those obtained via GFEM.

At Table 2 the maximum value of each type of displacement in Mindlin's plate theory is presented, as well as relative errors associated to each maximum displacement and distributed error based on the L_2-norm ($e^n_{\%}$).

Table 2. Displacements of FGM plate (Reissner-Mindlin) and associated errors in relation to analytical solution

Displac.	**Maximum**	$(\bar{x}, \bar{y})$	**Error disp. max(%)**	$\mathbf{e}^n_{\%}$**(%)**
$\bar{w}^o$	$3.78 \cdot 10^{-2}$	$(\frac{1}{2}, \frac{1}{2})$	$8.5 \cdot 10^{-8}$	$9.6 \cdot 10^{-6}$
$\bar{u}^o$	$1.91 \cdot 10^{-4}$	$(0, \frac{1}{2})$	$1.2 \cdot 10^{-6}$	$4.8 \cdot 10^{-5}$
$\bar{v}^o$	$1.91 \cdot 10^{-4}$	$(\frac{1}{2}, 0)$	$2.9 \cdot 10^{-6}$	$6.3 \cdot 10^{-5}$
ψ_x	$4.60 \cdot 10^{-5}$	$(0, \frac{1}{2})$	$1.2 \cdot 10^{-6}$	$4.8 \cdot 10^{-5}$
ψ_y	$4.60 \cdot 10^{-5}$	$(\frac{1}{2}, 0)$	$2.9 \cdot 10^{-6}$	$6.3 \cdot 10^{-5}$

By analyzing this data, it's possible to perceive that the GFEM model was able to accurately represent the deformed configuration of the FGM plate, producing very small errors (with order of magnitude of 10^{-4}%).

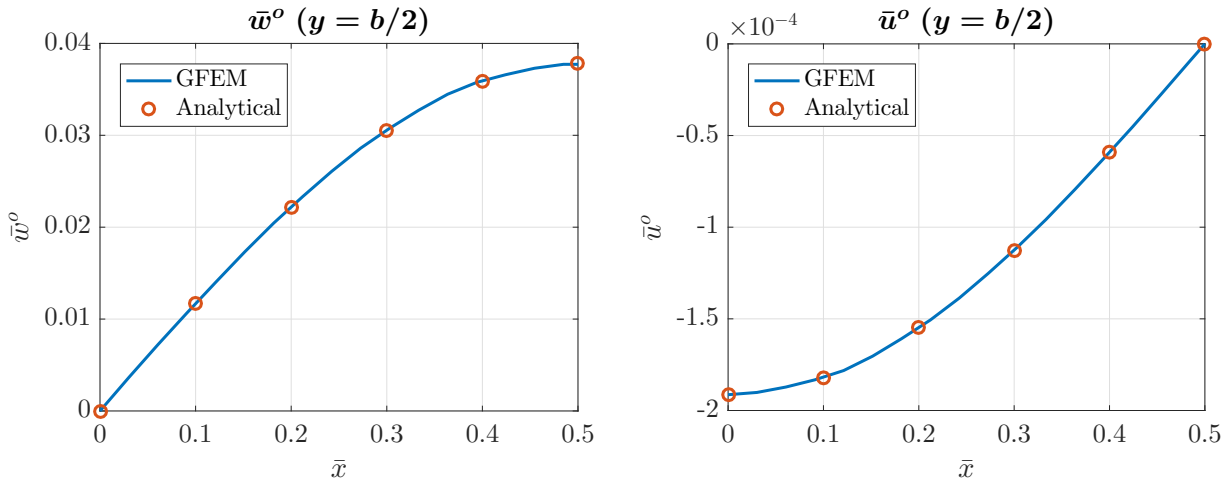

Figure 4. Displacements over x (behavior of v^o over y is similar to that of u^o over x)

4. CONCLUSIONS

The GFEM model developed by this work was capable of accurately representing the behavior of FGM plates acting under the simultaneous effect of stresses originated from harsh thermal gradients and mechanical loads. The incorporation of thermal conductivities' temperature dependence to the existing mechanical models of FGM plates allowed a more accurate representation of the structure's response and the developed theoretical and numerical advances were successfully validated through comparison with a reference analytical solution.

5. ACKNOWLEDGEMENTS

This work was funded by CNPq (Conselho Nacional de Desenvolvimento Científico e Tecnológico, Brazil) under grant number 146196/2021-0.

6. REFERENCES

Barcellos, C.S., Mendonça, P.T.R. and Duarte, C.A., 2009. "A ck continuous generalized finite element formulation applied to laminate kirchhoff plate model". *Comput Mech*, Vol. 44, pp. 377–393.

Bever, M.B. and Duwez, P.E., 1972. "Gradients in composite materials". *Materials Science and Engineerring*.

Koizumi, M. and Niino, M., 1995. "Overview of FGM research in japan". *MRS Bulletin*, Vol. 20, pp. 19–21.

Lee, Y., Zhao, X. and Reddy, J., 2010. "Postbuckling analysis of functionally graded plates subject to compressive and thermal loads". *Computer Methods in Applied Mechanics and Engineering*, Vol. 199, No. 25, pp. 1645–1653.

Mendonça, P.T.R., 2019. *Materiais compostos e estruturas sanduíche: projeto e análise*. Editora Orsa Maggiore, Florianópolis, Brasil, 2nd edition.

Park, J.S. and Kim, J.H., 2006. "Thermal postbuckling and vibration analyses of functionally graded plates". *Journal of Sound and Vibration*, Vol. 289, pp. 77–93.

Reddy, J.N., 1998. "Thermomechanical analysis of functionally graded cylinders and plates". *Journal of Thermal Stresses*, Vol. 21, pp. 593–626.

Reddy, J.N., 2000. "Analysis of functionally graded plates". *International Journal for Numerical Methods in Engineering*, Vol. 47, pp. 663–684.

Swaminathan, K. and Sangeetha, D., 2017. "Thermal analysis of fgm plates–a critical review of various modeling techniques and solution methods". *Composite Structures*, Vol. 160, pp. 43–60.

7. RESPONSIBILITY NOTICE

The authors are solely responsible for the printed material included in this paper.